Biofilms (2004) **1**, 1–15 © 2005 Cambridge University Press
DOI: 10.1017/S1479050505001560 Printed in the United Kingdom

A modelling study of the activity and structure of biofilms in biological reactors

J. B. Xavier*, **C. Picioreanu and M. C. M. van Loosdrecht**

* Corresponding author:
Dr J. Xavier
Department of Biotechnology
Delft University of Technology
Julianalaan 67
2628 BC Delft
The Netherlands
T 31 15 2781551
F 31 15 2782355
E J.Xavier@tnw.tudelft.nl

Department of Biotechnology, Delft University of Technology, Julianalaan 67, 2628 BC Delft, The Netherlands

ABSTRACT

In spite of the large range of morphologies observed for biofilms, there is strong experimental and theoretical evidence that the complex nature of biofilm structure dynamics is primarily a consequence of the effect of environmental conditions on biofilm development. It has been observed from the operation of industrial and laboratory-scale biofilm reactors that the structure of biofilms results from a balance of the detachment forces and the regimen of transport of a growth-limiting substrate. The overall performance of biofilm reactors is intrinsically dependent on biofilm morphology. The spatial distribution of the diverse dissolved and particulate components through the biofilm matrix and the shape of its external surface influence the rates of the occurring bioconversions, and structure also influences the stability of the biofilm in terms of resistance to mechanical stress. Individual-based modelling (IbM) of biofilms structure dynamics is used here to unify observations from the operation of biofilm reactors by simulating biofilm growth under variable detachment forces and mass transport regimens for a growth-limiting substrate. The IbM is a bottom-up approach, where the global system behaviour is derived from the local interactions of multiple elements acting independently. Transport and reaction of a solute species, local microbial growth rates and the effect of external detachment forces applied to the biofilm are modelled using differential approaches. Simulations carried out in two-dimensional space using this model illustrate a range of biofilm morphologies that emerge from different reactor operation parameters, reproducing trends observed experimentally. Comparison of multi-dimensional modelling results with those obtained using one-dimensional approaches enforces the need to use multi-dimensional modelling to predict properties that derive from the spatial biofilm structure.

INTRODUCTION

The large variety of biofilm structures observed in both natural and industrial biofilms is a manifestation of the complexity inherent in the attached microbial communities (Van Loosdrecht *et al.*, 1995). For particular biofilms, this complexity is reported to be a consequence of the complex behaviour of the organisms of which it comprises, such as the use of cell-to-cell signals (Davies *et al.*, 1998) or other behaviour associated with a "biofilm phenotype" (Stoodley *et al.*, 2002). However, it is often the case that the complexity of biofilm structure may be explained as a consequence of the heterogeneous composition of biofilms or of interactions between the various processes involved in biofilm formation. For example, the influence of signal molecules on biofilm structure was shown to be insignificant as a consequence of mass transfer effects in systems with significant flow (Purevdorj *et al.*, 2002). Heterogeneity may exist in biofilms at several levels: the distribution of microbial species in multi-species consortia; the spatial arrangement comprising substances such as active biomass, extracellular polymeric substances (EPS), inert and inorganic materials; the distribution of biomass clusters and pores, etc. The processes involved in biofilm formation, in turn, may generally be grouped as: (1) initial colonization, (2) growth, (3) attachment and (4) detachment of biomass (Bryers & Characklis, 1982).

Biofilm structure is of special importance in the operation of biofilm reactors. The density of a biofilm, for example, is a property that directly affects the efficiency of bioprocesses, as it defines the achievable biomass concentration in the reactor. Biofilm thickness is another important morphological feature. For aerobic processes, thin biofilms are desirable (Tijhuis *et al.*, 1996), as a consequence of the low depth of penetration of oxygen.

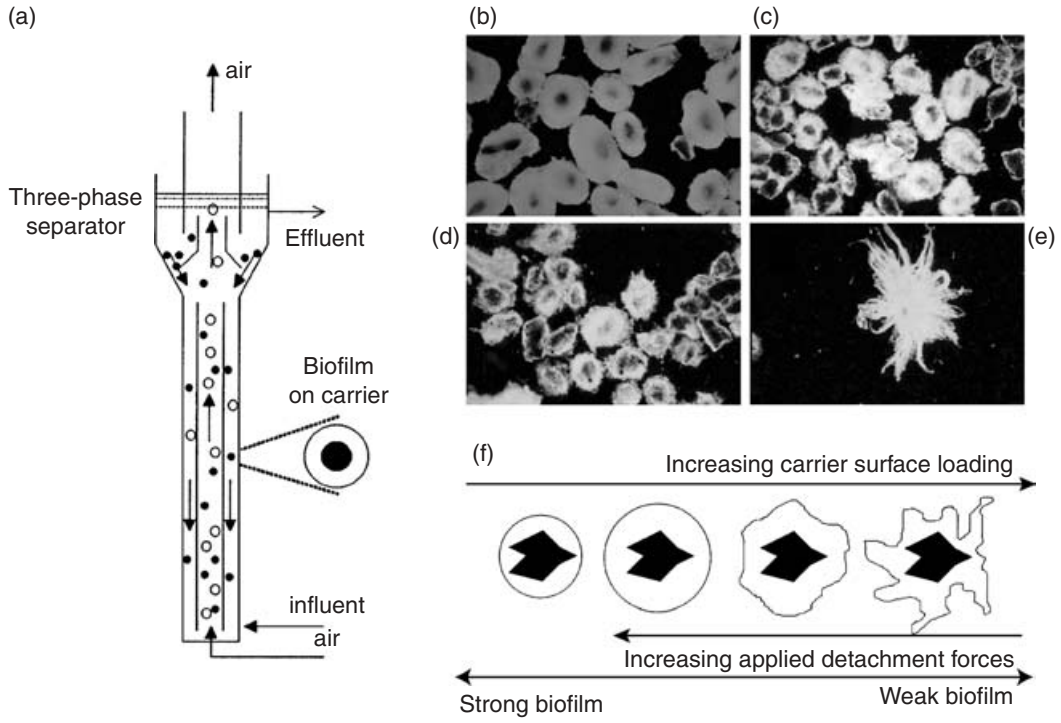

Fig. 1: Biofilm structure in the biofilm airlift suspension (BAS) reactor. (a) Schematic illustration of a laboratory-scale BAS reactor (Tijhuis *et al.*, 1994); (b to e) Structure of biofilms grown at different conditions in a laboratory-scale BAS reactor (Tijhuis *et al.*, 1996), ranging from smooth (b) to rough (e). Growth was carried out at the same substrate loading rates but with different shear conditions, thus producing different biofilm morphologies. (f) Illustration of the hypothesis (Van Loosdrecht *et al.*, 1995) that biofilm structure is defined by a balance between biofilm surface growth (resulting from the conversion yields and substrate transport regimens) and detachment processes (from Tijhuis *et al.*, 1996).

The fraction of voids in the biofilm shape, quantified by the parameter "porosity" (Lewandowski, 2000), also influences biofilm activity. Biofilm activity may also be affected negatively by roughness in the biofilm shape, an effect studied both experimentally (Wasche *et al.*, 2002) and by modelling approaches (Rittmann *et al.*, 1999; Picioreanu *et al.*, 2000; Klapper, 2004). In addition to biofilm activity, its mechanical stability also is influenced by the structure, as biomass detachment, the primary mechanism balancing microbial growth in steady-state systems, results from a combination of external forces applied on the biofilm and various internal processes (Stewart, 1993; Picioreanu *et al.*, 2001).

Biofilm airlift suspension (BAS) reactors used for the aerobic removal of organic carbon from waste water (Heijnen *et al.*, 1993) are very suitable for assessing the influence of growth and detachment conditions on biofilm structure. Inside these reactors, biofilms grow attached to small solid particles, providing a high area of carrier surface. The particles are homogeneously suspended in the reactor, ensuring homogeneous shear and substrate loading for the entire biofilm surface. Furthermore, because the shear acting on the biofilm is caused predominantly by particle–particle interactions (Gjaltema *et al.*, 1995), the influence of detachment forces may also be easily analysed by changing the concentration of solid particles in the reactor (Kwok *et al.*, 1998). Observations of diverse morphologies resulting from operating the BAS reactor under different conditions led to the hypothesis that the main determining factor for biofilm morphology is a balance between the conditions of biomass growth, usually limited by transport of a substrate, and the detachment of biomass (Van Loosdrecht *et al.*, 1995). Fig. 1 shows a schematic representation of the BAS reactor (panel a), examples of the diverse biofilm morphologies obtained from operating a laboratory-scale BAS reactor under different conditions (panels b, c, d, and f), ranging from smooth (panel b) to rough (panel e) morphologies for the biofilms growing attached to basalt particles, and a schematic representation of the relationship between biofilm morphology and strength as a function of the substrate surface loading and the applied detachment forces (panel f).

In order to accurately describe the bioconversions occurring in biofilm reactors, biofilm models must also account for the multiple physical processes occurring. Stratified one-dimensional (1D) models provide a good description of solute and biomass transport processes. A typical example is the well-established stratified multi-species model of Wanner and Gujer (Wanner & Gujer, 1986; Wanner & Reichert, 1996) implemented in the AQUASIM program (Reichert, 1994), for which numerous applications may be found in the literature. In spite of their wide acceptance among bioprocess engineers and their utility to describe overall bioconversions, 1D approaches are always limited to a range of operating conditions. The limitations appear evident when factors that result from the biofilm structure, such as external

mass transfer coefficients and biofilm porosity, have to be provided as input, rather than being derived from the model. To surpass these shortcomings, multi-dimensional models of biofilms (Picioreanu *et al.*, 2004b), which have been in development for the past seven years, aim to provide a description of biofilm activity and structure based on first principles.

In the present work, some of the experimentally observed trends in biofilm activity and structure are reproduced using a simple model of biofilm growth that considers a single heterotrophic bacterial species and a single solute species, oxygen. The factors influencing structural heterogeneity and its consequences in overall activity of the biofilm are considered, namely the effect of (a) applied erosion forces and (b) maximum specific growth rate of the organisms. Individual-based modelling (IbM; Kreft *et al.*, 2001; Picioreanu *et al.*, 2004a) was used here. Three-dimensional (3D) simulations of biofilm development, including multiple species and reactions involved, were already implemented using this approach (Picioreanu *et al.*, 2004b), but analysis of the results is complex and outside the scope of this study. By considering a very simple kinetic model of biofilm growth here, we focus on the effects of detachment versus the transport of a growth-limiting substrate, in our case oxygen. Results from these 2D simulations are further confronted with results from two 1D approaches: a steady-state model based on zero-order kinetics (Pérez *et al.*, 2004) and a dynamic model based on Monod kinetics implemented in AQUASIM (Reichert, 1994). The steady-state zero-order model is solved analytically and therefore is very useful for analysing trends directly, whereas the dynamic model with Monod kinetics is used for accessing deviations from the zero-order case. Results from these modelling approaches, consisting of three levels of model sophistication, are used here as basis for discussion of established views about the influence of environmental conditions on biofilm structure and activity.

MODEL SYSTEM DESCRIPTION

The model system considered here is a simplification of a biofilm reactor consisting of a biofilm phase and liquid phase. The following assumptions are considered:

1. The biomass in the biofilm has uniform density and biomass growth is described by Monod kinetics as a function of oxygen, the growth-limiting solute.
2. The bulk liquid is completely mixed and bulk oxygen concentration is constant in time.
3. In the biofilm and in the concentration boundary layer, mass transport of the dissolved substrate (oxygen here) occurs by diffusion.
4. Biomass detachment is a second-order function of the distance to the solid surface (x), which guarantees the existence of a steady state (Stewart, 1993).

$$F_{\mathrm{det}} = k_{\mathrm{det}} x^2 \qquad [\mathrm{LT}^{-1}] \tag{1}$$

Here, F_{det} is the detachment speed function, i.e. the speed at which the biofilm front will retract as a consequence of the biomass detachment. The detachment rate coefficient, k_{det}, has dimensions of $\mathrm{L}^1\mathrm{T}^{-1}$.

The system comprises a single particulate species (heterotrophic biomass) and a single solute species, oxygen. The kinetic expressions used for biomass formation and oxygen consumption are

$$R_{\mathrm{H}} = \mu^{\max} \frac{C_{\mathrm{O}}}{C_{\mathrm{O}} + K_{\mathrm{O}}} C_{\mathrm{H}} \qquad [\mathrm{M_H L^{-3} T^{-1}}] \tag{2}$$

$$R_{\mathrm{O}} = -Y_{\mathrm{OH}} R_{\mathrm{H}} \qquad [\mathrm{M_O L^{-3} T^{-1}}] \tag{3}$$

where R_{H} is the biomass production rate, $\mu^{\max}$ is the maximum specific growth rate, C_{O} is the concentration of oxygen, R_{O} is the reaction rate of oxygen and Y_{OH} is the yield (in grams) of consumed oxygen per gram of COD (chemical oxygen demand) of biomass produced. The value of R_{O} will be negative here, since oxygen is consumed only in the process of biomass production. The substrate mass balances include transport by diffusion (described by Fick's second law) and a biological reaction in the biofilm only. For the steady state this is:

$$D_{\mathrm{O}} \nabla^2 C_{\mathrm{O}} + R_{\mathrm{O}} = 0 \quad \text{in the biofilm} \qquad [\mathrm{M_O L^{-3} T^{-1}}] \tag{4}$$

$$D_{\mathrm{O}} \nabla^2 C_{\mathrm{O}} = 0 \quad \text{in the concentration boundary layer} \qquad [\mathrm{M_O L^{-3} T^{-1}}] \tag{5}$$

where D_{O} is the value of the molecular diffusivity of oxygen. The parameters used in the model are listed in Table 1.

STEADY-STATE SOLUTIONS FOR 1D MODELS

One-dimensional descriptions neglect heterogeneity in the biofilm in the directions parallel to the solid substratum and, therefore, assume a homogeneous planar biofilm shape. Only gradients in direction x, perpendicular to the solid substratum surface, are considered. The biofilm thickness at the steady state ($L_{\mathrm{f,ss}}$) is reached when detachment equals the overall biomass production in the biofilm. This is described by the following equation, defined in terms of the velocity of the biofilm front:

$$\int_0^{L_{\mathrm{f,ss}}} \frac{R_{\mathrm{H}}}{C_{\mathrm{H}}} \, \mathrm{d}x = k_{\mathrm{det}} L_{\mathrm{f,ss}}^2 \qquad [\mathrm{LT}^{-1}] \tag{6}$$

Here, the advancement speed of the front resulting from biomass growth (left-hand side of equation 6) equals the front retreat speed resulting from detachment occurring at the biofilm–liquid interface (right-hand side of equation 6). The detachment speed is obtained from equation 1 using $L_{\mathrm{f,ss}}$ for the value of x. Although no analytical solution exits for the set of partial differential equations defining the system if Monod kinetics is considered for R_{H} (equation 2), solutions exist if either zero-order kinetics (valid for high concentrations of oxygen, i.e. when $C_{\mathrm{O}} \gg K_{\mathrm{O}}$) or first-order kinetics (valid for low concentration of oxygen, i.e. when $C_{\mathrm{O}} \ll K_{\mathrm{O}}$) are assumed (Levenspiel, 1972). Other alternatives consist in using an average of the zero- and first-order solutions (Pérez *et al.*,

Table 1: Parameters used in models. Values of k_{det} are changed for the results presented in the section "Influence of imposed detachment on the steady state of biofilm". Values of μ^{max} are changed for the results presented in the section "Influence of maximum specific growth rate on the steady state of biofilm"

Parameters	Description	Value	Units	Notes/references
Solute species				
C_O^{bulk}	Bulk concentration	0.004	gO L^{-1}	
D_O	Diffusivity	8.3×10^{-6}	$m^2\ h^{-1}$	Rittmann *et al.*, 2004
Particulate species				
ρ_H	Specific mass of heterotrophic biomass	200	gCOD-H (L particle)$^{-1}$	
Yield coefficients				
Y_{OH}	Yield of oxygen on produced biomass	0.505	gO gCOD-H^{-1}	Beun *et al.*, 2002
Processes				
μ^{max}	Maximum specific growth rate of micro-organisms	0.47 (except where noted)	gCOD-H gCOD-H^{-1} h^{-1}	Beun *et al.*, 2002
K_O	Saturation constant	3.50×10^{-4}	gO L^{-1}	Rittmann *et al.*, 2004
k_{det}	Detachment rate coefficient	9.5 (except where noted)	$m^{-1}\ h^{-1}$	
Computation parameters				
System size 2D		4000×4000	μm^2	For 2D simulations
$R_{division}$	Maximum particle radius	6	μm	
L_{bl}	Boundary layer thickness	200	μm	
L_z	Depth of system	30	μm	
Δx	Grid element size	30	μm	For 2D simulations

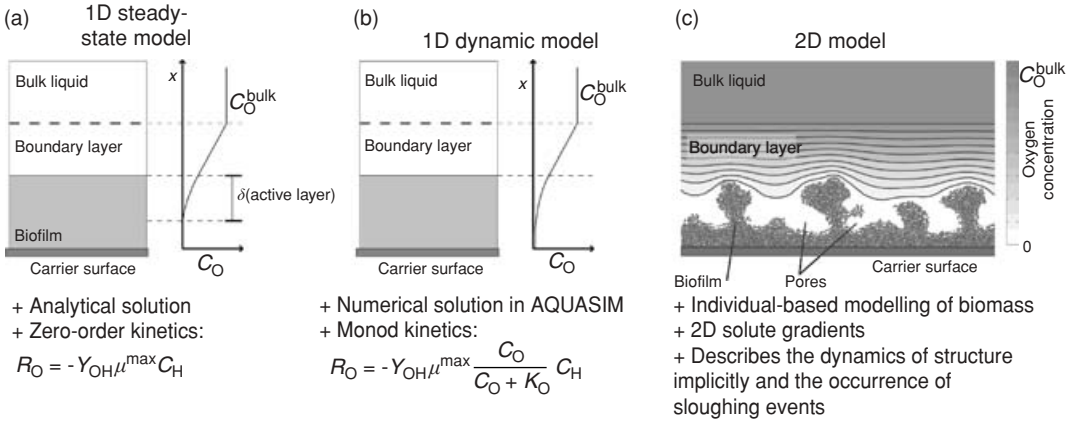

Fig. 2: Modelling approaches used in the present study: (a) 1D steady-state model with zero-order kinetics for biomass growth and oxygen consumption solved analytically; (b) 1D dynamic model with Monod-type kinetics, solved numerically using the AQUASIM program (Reichert, 1994); (c) 2D model solved using individual-based modelling.

2004), pseudoanalytical methods (Saez & Rittmann, 1992), or numerical solutions (e.g. Wanner & Gujer, 1986). Assuming zero-order kinetics provides the simplest solution. When growth is zero-order for the concentration of oxygen, a critical depth exists, the oxygen penetration depth (δ), below which the oxygen concentration is zero. The existence of an oxygen penetration depth δ is illustrated in Fig. 2a. The value for δ may be determined analytically from the model parameters as explained in the Appendix. There, k_L is the external mass transfer coefficient defined according to film theory from a concentration boundary layer of thickness L_{bl} and the value of the molecular diffusivity of oxygen, D_O, according to:

$$k_L = \frac{D_O}{L_{bl}} \qquad [LT^{-1}] \qquad (7)$$

For this zero-order approximation, the value of δ, together with the detachment expression (equation 1) immediately defines all steady-state biofilm properties (for a list of some properties directly derived from δ, see Appendix, Table 3). The zero-order approximation is useful to illustrate the importance of the relative rates of reaction and diffusion and of external mass transfer properties, reflected in parameters such as the Thiele modulus (ϕ_O, a dimensionless number reflecting the ratio of reaction rate of a solute and the external mass transfer rate of that solute, defined in Appendix, equation 17), in determining the oxygen penetration and, hence, the steady-state properties of the biofilm. Deviations from the zero-order approximation are estimated to be less than 10% when $C_O^{bulk} > 2.5K_O$ (Pérez *et al.*, 2004). The 1D solution for Monod kinetics, as obtained from numerical

simulation carried out using the AQUASIM program, is also considered here for the purpose of evaluating deviations from the zero-order approximation. This constitutes the second modelling approach used here, represented schematically in Fig. 2b.

2D SIMULATIONS FROM INDIVIDUAL-BASED MODELLING

Two-dimensional simulations were carried out using IbM, represented schematically in Fig. 2c. IbM is a bottom-up approach where the dynamics of a community is derived from the actions and interactions of the individuals of which it is composed. The IbM was applied previously to biofilm modelling (Kreft *et al.*, 2001) and present applications include the modelling of several multi-species biofilm systems and activated sludge flocs (for an overview of recent applications of the IbM, see Picioreanu *et al.*, 2004b). Numerical details of the IbM used here may be found in Picioreanu *et al.* (2004a). In this paper, only a brief description will be provided.

In 2D applications of the IbM, biomass is represented as being composed of particles with a circular shape. These particles, called "agents", are entities with an internal state, defined in this paper by biomass, size and location in space. The size (radius, R_p) of a particle is related to its biomass (M_p) through the value of ρ_H, the specific mass of heterotrophic biomass

$$R_p = \sqrt{\frac{M_p}{\rho_H 2\pi L_z}} \qquad [L] \qquad (8)$$

In equation 8, L_z is the depth of the system along a third dimension, used to provide biomass particles (i.e. agents) with a volume, for mass conservation purposes. Agents follow behaviour rules that mimic the behaviour of a bacterial cell: they grow by intake of nutrients; divide, creating an offspring agent; and move (in continuous spatial coordinates) when pushed by neighbouring agents. Growth (biomass production) of an agent is a function of the local concentration of oxygen, following a variation of equation 2 written in terms of biomass per particle

$$\frac{dM_p}{dt} = \mu^{max}\frac{C_O}{C_O + K_O}M_p \qquad [M_H T^{-1}\ \text{particle}^{-1}] \qquad (9)$$

Diffusion–reaction of the solute species (oxygen) is modelled using an uncoupled approach (Picioreanu *et al.*, 1998), where solute concentration fields are described using a rectangular grid. In the simulations shown here, a grid of 129 × 129 grid nodes was used for the oxygen concentration fields.

Simulations carried out in the IbM use a computational cycle that consists of the sequential execution of operations that represent the processes involved in biofilm development. Here, the computational cycle proposed previously (Picioreanu *et al.*, 2004a) was simplified for the case where no biomass decay is considered and the bulk concentration of oxygen (C_O^{bulk}) is kept constant throughout the simulation. This means that no mass balances to the bulk liquid are executed, and concentration gradients exist only in the concentration boundary layer and in the biofilm matrix. The operations executed in one iteration of the simulation cycle, corresponding to a period of time Δt, are the following:

1. Growth and division of biomass.
2. Spreading of the biofilm matrix.
3. Detachment of biomass.
4. Updating of local solute concentrations by solving diffusion–reaction mass balances to pseudoequilibrium.
5. Advancement of the present simulation time (t) to $t+\Delta t$ and return to step (1) to start a new iteration of the cycle, or stop the iteration if t reached the predefined simulation finishing time, t_{finish}.

These steps of the simulation cycle are represented schematically in Fig. 3.

The method used for implementing biomass detachment follows a continuous description of biomass erosion that uses a detachment function F_{det}. In this method, the speed of a point $\boldsymbol{x}$ located at the biofilm/liquid interface (here called Γ) that results from the erosion of the biofilm is given by:

$$\frac{d\boldsymbol{x}}{dt} = -F_{det}(\boldsymbol{x})\boldsymbol{n}(\boldsymbol{x}) \qquad [LT^{-1}] \qquad (10)$$

where $F_{det}(\boldsymbol{x})$ is the value of the detachment speed function at that point and $\boldsymbol{n}(\boldsymbol{x})$ is the vector normal to the biofilm surface at point $\boldsymbol{x}$. Using this method, it is found that local detachment rates are dependent on the local curvature of the biofilm interface Γ, being higher where the surface is convex (such as the tips of finger-like clusters) and lower where the surface is concave (such as the interior of pores in the biofilm). By substituting the detachment speed function defined in equation 1, equation 10 becomes:

$$\frac{d\boldsymbol{x}}{dt} = -k_{det}x^2\boldsymbol{n}(\boldsymbol{x}) \qquad [LT^{-1}] \qquad (11)$$

This equation is solved numerically at step 3 of each iteration of the simulation cycle using the fast level set method (Sethian, 1996). This method allows discrete detachment events that derive from random instabilities in the surface, i.e. biomass sloughing, to be implicitly derived from the simulations, by removing biomass that becomes disconnected from the biofilm (as shown in the transition of panel d to panel e in Fig. 3). Erosion and sloughing are modelled in this way using the same mechanism, producing results equivalent to those obtained using a mechanistic method of fluid-induced detachment in a 2D biofilm model (Picioreanu *et al.*, 2001). In spite of its simplicity, the method used here is preferable to the referred mechanistic method for the purpose of the present work, since it allows similar results yet is significantly less computationally demanding. Details of the numerical nature of the method used here to model detachment are not within the scope of the present paper (J. B. Xavier *et al.*, unpublished results).

The simulations in 2D were performed starting from an initial inoculum consisting of a thin homogeneous layer of microorganisms covering a planar surface of attachment.

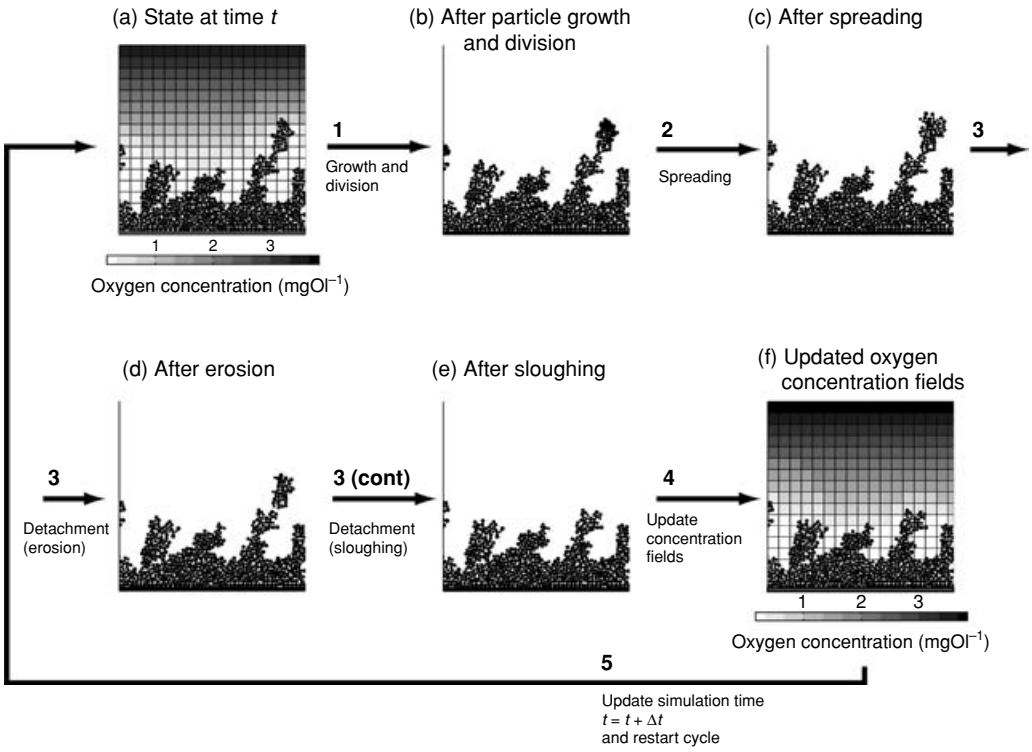

Fig. 3: Schematic representation of the simulation cycle used in the individual-based modelling approach for the 2D simulations. A detailed description of the simulation cycle of the procedures illustrated here is provided by Picioreanu *et al.* (2004a). (a) The state at the beginning of the simulation cycle, with solute concentration fields computed for a 2D grid space discretization. Biomass particles (agents) grow according to the local oxygen concentration, following equation 9. Here, owing to the sharp gradients of oxygen formed, only the particles located at the tips of finger-like structures (where oxygen concentration is higher) will grow significantly. (b) After growth and division. Particle division occurs whenever particle radius grows above a critical value ($R_{division}$), giving rise to an offspring particle. (c) Growth and division originate overlapping of biomass particles. This overlap is undone via a spreading procedure that results in a slight advancement of the biofilm front, as shown here. (d) The first step in detachment is erosion, i.e. removal of biomass from the biofilm surface, according to equation 11. (e) The second step in detachment is sloughing, i.e. the removal of clusters of biomass that become disconnected to the remaining biofilm. (f) Once the new biofilm structure is defined, the oxygen concentrations are updated by solving the diffusion–reaction equations in 2D. The sloughing of a tall biofilm feature, as occurred here, results in a local increase in the penetration of the dissolved oxygen into the biofilm. This shows that the occurrence of sloughing events increases bacterial growth in the deeper regions of the biofilm.

Simulations were carried out long enough to assure that a "steady state", following the definition presented below, was achieved and to allow the meaningful determination of time-averaged values of the steady-state biofilm. Animations of the 2D simulations analysed here may be obtained from our website in the form of digital video files. Also, an interactive demonstration of the computer program used here for the IbM 2D simulations is available. The website may be accessed via the URL: <http://www.biofilms.bt.tudelft.nl/reactorsPaperMaterial/>.

RESULTS

Steady state derived from 2D simulations

Biofilm development is a stochastic process. In experimental settings, biofilm structures are very difficult to reproduce (Heydorn *et al.*, 2000; Jackson *et al.*, 2001; Lewandowski *et al.*, 2004). This is an issue of key importance for the design of biofilm monitoring experiments. Lewadowski *et al.* (2004) observed that biofilms grown flat in plate reactors were reproducible up to the occurrence of a first sloughing event, after which structure dynamics became unpredictable. Since the 2D model used here includes the occurrence of sloughing events, it is necessary to address the reproducibility of simulations and the existence of a true steady state. For simulations where detachment by sloughing constitutes a significant fraction of the total detached biomass, the biofilm structure will never reach a true steady state, as reported by Lewadowski *et al.* for their experiments. However, in long-term biofilm growth, a "noisy" steady state can emerge, even for cases where sloughing events occur significantly, as postulated by Morgenroth & Wilderer (2000). Characteristic of this "noisy" steady state is that the long-term net biofilm accumulation rate becomes close to nil, while the remaining biofilm properties are noisy (fluctuate with time) but keep within a steady deviation range around their mean value. The IbM simulations carried out here use a random number generator for three operations: (1) the placement of inoculum biomass particles, (2) the distribution of biomass at particle division (to reduce the probability of synchronized division of all the biomass agents) and (3) the orientation for placement of particles upon division. As simulations reported here start with

Table 2: Steady-state biofilm properties for five replicates of 2D simulation runs ($k_{det} = 9.5\,m^{-1}\,h^{-1}$). Values shown are averages from day 50 until end of simulation at day 166, with confidence intervals of ± 2 (standard deviations). Accumulation rates are very close to zero, especially when compared with the magnitude of detachment and biomass production rates, which confirms that a "noisy" steady state is achieved. The five replicates show good agreement both in the average values of steady-state properties and in their standard deviations

	Steady-state property						
Replicate	Thickness L_f (μm)	Porosity ε	Total detachment rate (gCOD m^{-2} day^{-1})	Erosion rate (gCOD m^{-2} day^{-1})	Sloughing rate (gCOD m^{-2} day^{-1})	Biomass production rate (gCOD m^{-2} day^{-1})	Accumulation (production – detachment) (gCOD m^{-2} day^{-1})
1	463.1 ± 83.1	0.53 ± 0.09	81.2 ± 170.6	61.2 ± 26.3	20.0 ± 170.2	82.7 ± 14.9	1.5
2	461.1 ± 85.5	0.53 ± 0.11	79.8 ± 151.4	59.2 ± 18.4	20.6 ± 152.2	80.2 ± 13.6	0.5
3	468.7 ± 65.2	0.55 ± 0.07	79.0 ± 157.2	58.5 ± 16.6	20.5 ± 158.1	78.8 ± 12.3	−0.1
4	472.2 ± 70.0	0.57 ± 0.07	77.2 ± 148.5	57.6 ± 18.2	19.6 ± 149.3	77.4 ± 11.5	0.2
5	460.0 ± 81.6	0.55 ± 0.09	79.4 ± 158.3	58.6 ± 23.3	20.8 ± 158.9	80.3 ± 12.7	0.9

inoculae that uniformly cover the surface of attachment, the effect of random inoculation is not very significant. The use of random numbers in particle division is also not significant in the long run, because redistribution of biomass in new particles after division averages 50% of that of the dividing particle and also all directions for division have equal probability. However, even the small changes occurring will alter the outcome of the simulation. Consequently, if different seeds of the random number generator are used, the same structure is never reproduced, as is also observed in experimental systems (Heydorn *et al.*, 2000).

In order to analyse the reproducibility of overall steady-state properties derived from simulations, five replicate 2D model runs were carried out using the same set of parameters but different seeds for the random number generator. Fig. 4 shows the results obtained from these five replicate simulations, carried out at $k_{det} = 3.2\,m^{-1}\,h^{-1}$ (the remaining parameters are listed in Table 1) and simulating 166 days of biofilm development. The time course of biofilm thickness, L_f, shown in Fig. 4a, reveals that simulations were in good agreement until the occurrence of the first sloughing events around day 30. Fig. 4b and c show biofilm structures for the five replicates at day 2 and day 8, respectively. In spite of some variability in the biofilm structure, more evident at day 8 than at day 2, areal porosity profiles show a very similar distribution of the biomass along the biofilm depth. The first sloughing events resulted in sudden decreases in the values of L_f for all the simulations. This first sloughing occurred at different times around day 40 for each of the five replicate simulations. After that, the structure of the biofilm and the exact occurrence of subsequent sloughing events were not precisely reproducible. In the period from day 50 until the end of the simulations at day 166, the biofilm thickness fluctuated around 460 μm, and the structures observed were visibly different between replicates. The structures obtained for the five replicates at day 100 and day 164 are shown in Fig. 4d and e, respectively. Not only are the structures visibly different between replicates but the distribution of the biomass along the biofilm depth (pictured in the areal porosity profiles) also is notably different. Furthermore, this variability occurred, even within the same replicate, throughout time. This is observed by comparing structures at day 100 and day 164 for the same replicate. In spite of this variability, a "noisy" steady state was achieved after day 50. This was observed as the long-term average biofilm accumulation rate was very close to zero for all replicates (values shown in Table 2). Values for the steady-state biofilm properties (thickness, porosity, total detachment rate, erosion rate, sloughing rate and biomass production rate), as well as their deviations, are also given in Table 2. These steady-state values, obtained from the time average of the properties for the 50–166 day period, show a good agreement for the five replicates. This demonstrates that, indeed, the "noisy" steady state of the simulated biofilm is reproducible in terms of overall biofilm properties, in spite of the fact that the structures obtained are not exactly the same.

Influence of imposed detachment on the steady state of the biofilm

Results from 2D simulations obtained for the same biofilm grown under different erosion forces (k_{det} was varied) are compared here with the 1D approaches described above, i.e. zero-order steady-state analytical solution and numerical solution of Monod kinetics. Fig. 5 shows the time course of biofilm thickness (L_f) obtained using the 2D model (IbM simulations) and the 1D dynamic model (simulations performed using AQUASIM). In Fig. 6 is shown an evaluation of the steady-state results from 1D and 2D models. Fig. 6a shows that, for 1D solutions, increasing the value of k_{det} produces thicker biofilms than those obtained from 2D simulations. Concerning the other biofilm properties shown (steady-state porosity (Fig. 6b), biomass production rate (Fig, 6c) and biomass detachment rate (Fig. 6d)), the analytical zero-order solution and Monod kinetics 1D models (grey and black lines, respectively) produce almost identical results. These results are, however, generally different from the results obtained from 2D simulations (data represented by the open symbols). Most notably, the divergence between results from 1D and 2D models increases for the cases

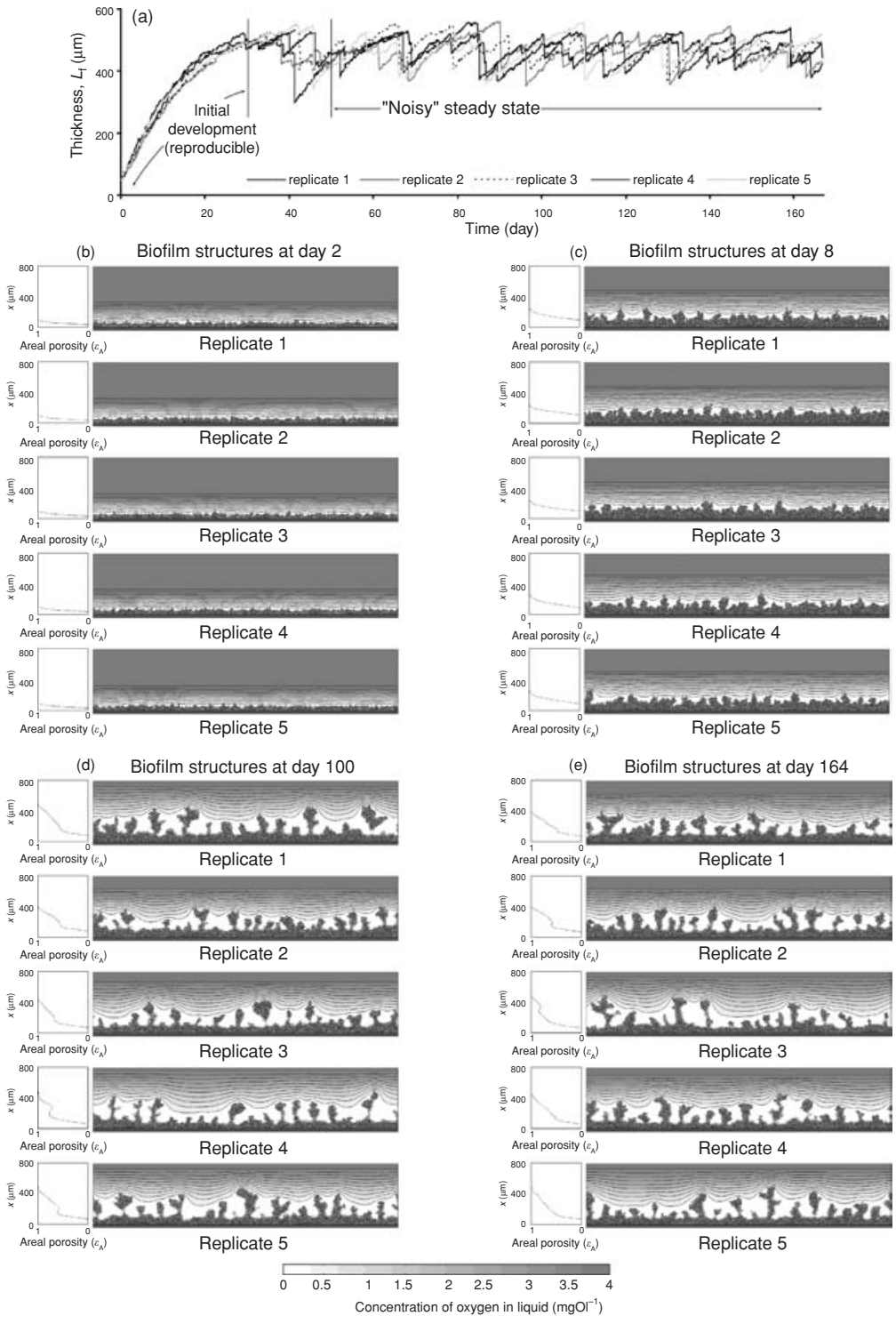

Fig. 4: Results for five replicates of a 2D simulation carried out at $k_{det} = 3.2$ m^{-1} h^{-1}. (a) Time course of biofilm thickness for the five replicates. Thickness (L_f), here defined as the height of the tallest point in the biofilm, shows sudden decreases resulting from sloughing events. Good agreement between replicates is observed for the initial biofilm development until the occurrence of the first sloughing event, after which the exact location of the biofilm front is apparently unpredictable. In spite of the biofilm never reaching a true steady value, after 50 days a "noisy" steady state is reached for all replicates (see text for details). (b to e) Biofilm structures for the five simulation replicates at 2, 8, 100 and 164 days of biofilm growth. Computed 2D gradients of oxygen are shown, as well as the vertical profile of biofilm areal porosity, ε_A, defined as the ratio between void volume and the total volume, comprising voids and biofilm.

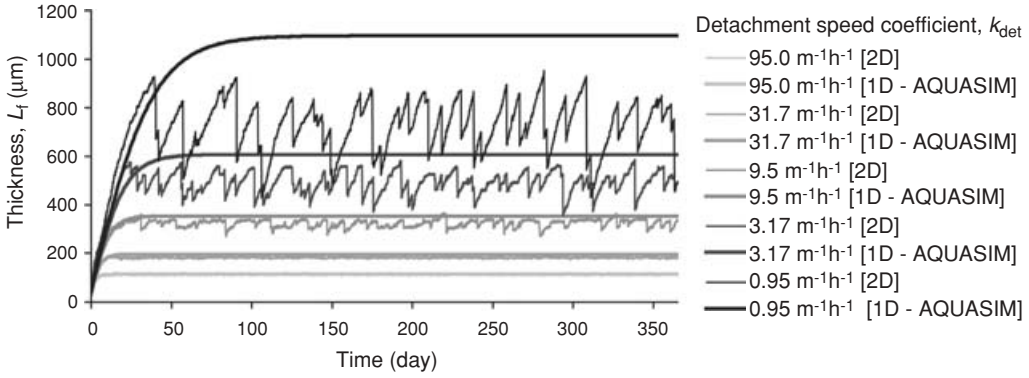

Fig. 5: The evolution of biofilm thickness (L_f) in time resulted from simulations carried out at different applied erosion forces. k_{det} values ranged from 0.95 to 95 m^{-1} h^{-1}. Thick lines indicates thickness obtained from 1D dynamic model using Monod kinetics and the 2D model results are shown by thin lines. 2D simulation results range from approximately constant L_f values for high applied erosion forces to very noisy L_f values observed at low applied erosion forces. 1D simulation results show good agreement with 2D simulations when applied erosion forces are high, but the two modelling approaches progressively diverge for the cases where applied erosion is low.

where k_{det} is lower. This is justified by the fact that the 2D model generates more porous biofilms at lower erosion rates, i.e. lower k_{det} (the steady-state porosity values are shown in Fig. 6b). For the lower k_{det} cases, tall finger-like structures were obtained (as seen in Fig. 6e for the cases with lowest k_{det}). This trend had already been reported in a modelling study that used a mechanistic representation of biomass detachment (Picioreanu *et al.*, 2001) and is in agreement with the experimental observations of Kwok *et al.* (1998). Other modelling studies (Eberl *et al.*, 2000; Picioreanu *et al.*, 2000; Klapper, 2004) and experimental evidence (Wasche *et al.*, 2000) indicate that roughness in the biofilm structure negatively influences the biofilm activity by increasing the external mass transfer resistance. The results from the 2D simulations shown in Fig. 6c (data represented by open squares) illustrate this trend, demonstrating a decrease in biofilm activity (here defined as the rate of biomass production) for the simulations carried out at lower k_{det} values. This effect of decreasing biofilm activity with decreasing k_{det} is, however, not visible in the steady-state 1D model (grey line) and only very slight in the 1D dynamic model (black line). This is a consequence of the inability of these 1D models to derive the heterogeneity in the biofilm structure, and its consequent effects on the external mass transfer resistance, that is patent in 2D models and the experimental results of Wasche *et al.* (2000). Two-dimensional simulations further predict that erosion is the most significant component of detachment for simulations carried out at high k_{det}, whereas at low k_{det} sloughing also constitutes a significant part of the detachment. This can be seen from the steady-state values of biomass detachment rate, shown in Fig. 6d. These data illustrate that, in spite of the decrease of total detachment rate (represented by open squares) with decreasing k_{det}, the sloughing rate (represented by black squares) increases with decreasing k_{det}. The occurrence of sloughing events is not predictable by 1D models. The 1D models used here consider only erosion, therefore it is logical that the results will deviate when sloughing becomes more important. Clearly, 2D biofilm models are needed to properly implement the detachment mechanisms and to be able to predict steady-state biofilm thickness.

Influence of maximum specific growth rate on the steady state of the biofilm

The effect of microbial growth rate on the steady state of the biofilm was also evaluated by performing simulations and keeping all parameters constant with exception of μ^{max}, which was varied from 0.05 to 0.54 h^{-1}. Applied erosion was here kept constant at $k_{det} = 9.5\ m^{-1}\ h^{-1}$. Results for steady-state properties resulting from application of the 1D and 2D models are shown in Fig. 7, as well as biofilm structures obtained from the 2D model at the end of the simulations (day 166), shown Fig. 7e. The value for the steady-state biofilm thickness (shown in Fig. 7a) was not altered by any change in the value of the μ^{max}, a result for which 1D and 2D models are in agreement. This is explained by the fact that μ^{max} influences biofilm steady-state accumulation through two opposing effects. Higher μ^{max} will increase the effect of diffusion limitation, resulting in decreased oxygen penetration and consequently in a thinner active layer (δ) in the biofilm. At the same time, this is compensated for by the fact that the biomass in the active layer will grow more rapidly. Fig. 7b shows that, for 2D simulations, higher μ^{max} produces a more porous biofilm. This is in agreement with experiments performed in BAS reactors showing that biofilms grown on substrates that allow faster growth rates lead to more porous structures (Villaseñor *et al.*, 2000). Biofilm heterogeneity, reflected in a higher porosity, also has consequences in the biofilm activity (rate of biomass produced) and in the biomass detachment from the biofilm. From 2D simulations, the rate of produced biomass is significantly lower when μ^{max} is higher (2D data are represented by open squares in Fig. 7c). The total biomass detachment rates show a similar trend, also for 2D (open squares in Fig. 7d). As in the previous case (i.e. the simulation results shown in Fig. 6d), 2D simulations predict that the relative contribution of sloughing to the

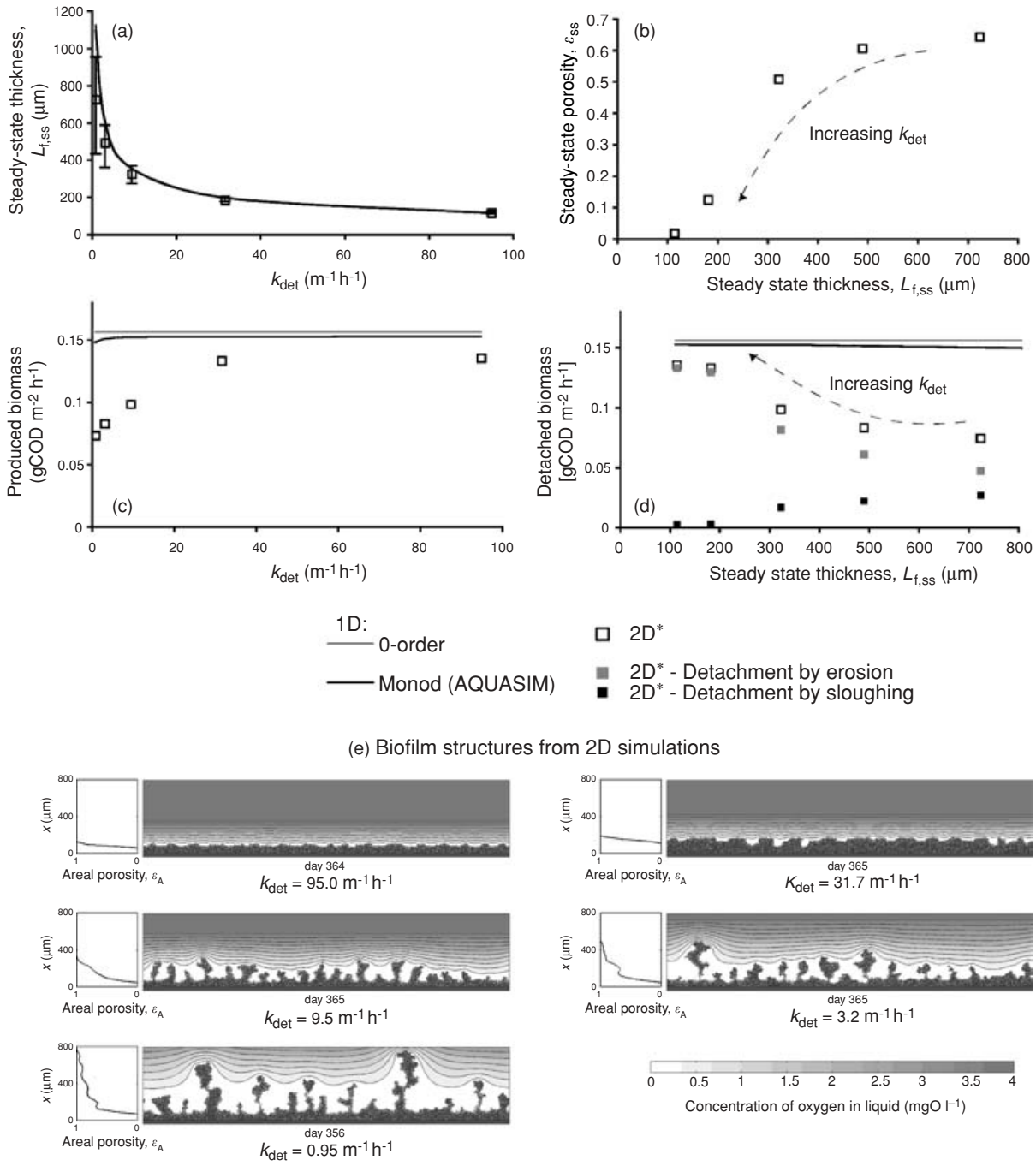

Fig. 6: Steady-state biofilm properties for the same biofilm but grown at a range of erosion forces (k_{det} varied from 0.95 to 95 m^{-1} h^{-1}). Data from five 2D simulations (* indicates data taken from Xavier *et al.* (2004)) is compared with results of two 1D models, (1) analytical solution from a steady-state model considering zero-order kinetics and (2) numerical solution from a dynamic model considering Monod kinetics. (a) Biofilm steady-state thickness, $L_{f,ss}$. For 2D simulations (data represented by open squares), error bars display the range between maximum and minimum thickness observed in the course of the simulated steady-state period. (b) Biofilm porosity, ε, at steady state versus the steady-state thickness for 2D simulations. For 1D cases porosity is always zero, since by definition the models assume a smooth and planar morphology of the biofilm. Therefore values for porosity of 1D cases are not shown in this plot. (c) Average rate of biomass production at the steady state. The 2D model predicts a significant increase of biomass production rate with increasing k_{det}, a trend that is not predicted by 1D models. (d) Biomass detachment rate ($R_{det,ss}$) versus the steady-state thickness. For 2D simulations, which also describe the occurrence of sloughing, the rates of detachment by erosion ($R_{ero,ss}$) and sloughing ($R_{slo,ss}$) are also presented. (e) Biofilm structures generated by the 2D model at the end of the simulations (day 365) for the five simulations carried out.

overall biomass detachment is higher for more heterogeneous biofilms (sloughing rate is represented by black squares in Fig. 7d), those produced by the biofilms with higher μ^{max} values. Results show again that as sloughing becomes more significant the difference between 1D and 2D solutions increases.

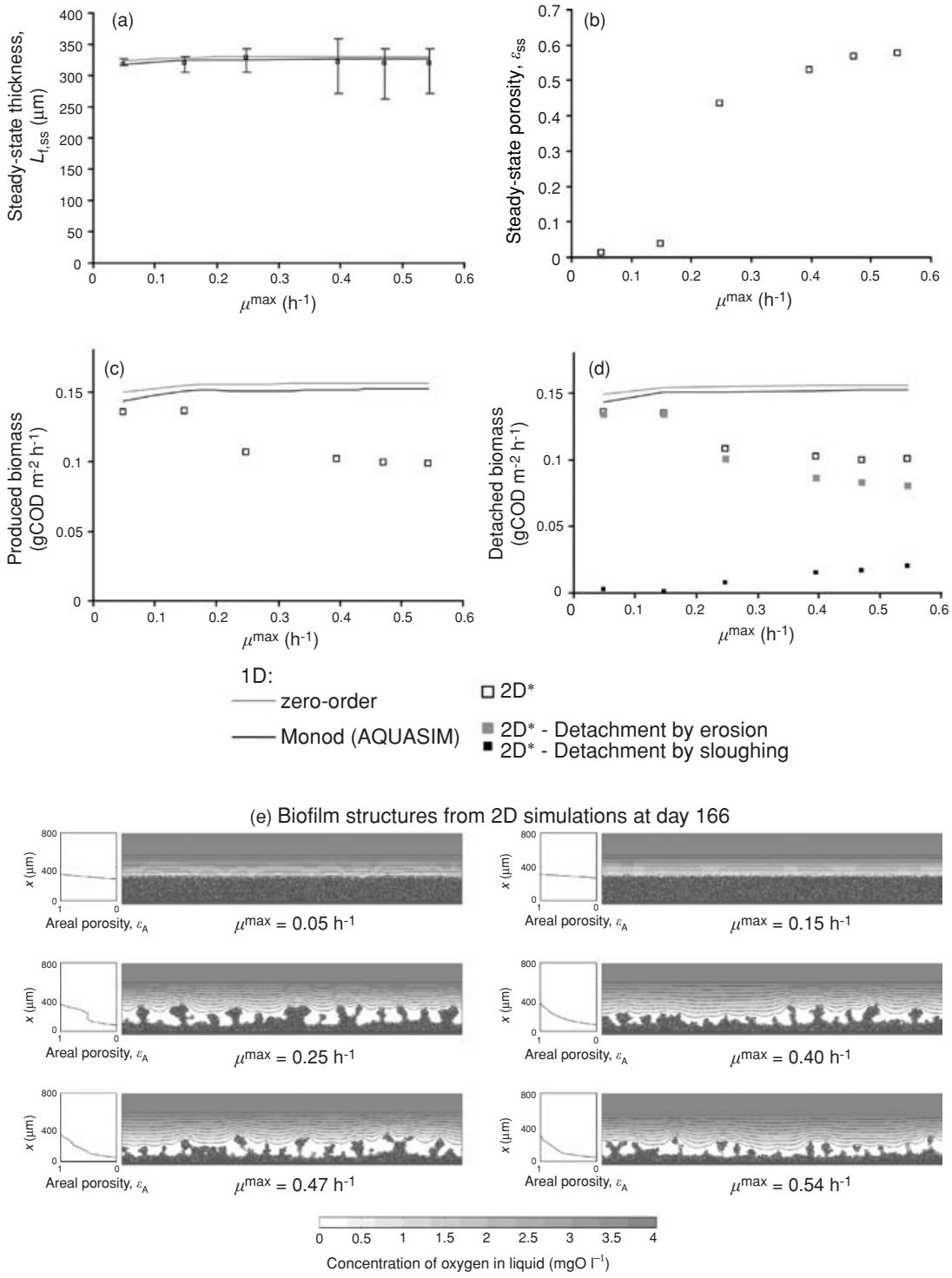

Fig. 7: Results from simulations carried for a range of values of μ^{max} from 0.05 to 0.54 h^{-1} and constant applied detachment, k_{det} = 9.5 m^{-1} h^{-1}. (a) Steady-state biofilm thickness. (b) Steady-state porosity, ε_{ss}, from 2D simulations (ε = 0 for the 1D models presented here). (c) Rate of biomass production. (d) Rate of biomass detachment, showing also rates of detachment by erosion and sloughing from 2D simulations. (e) Biofilm structures generated by the 2D model at the end of the simulations (day 166).

DISCUSSION

Biofilm steady state

The issue of the existence of a steady state was addressed here by performing five replicates of a simulation using a set of parameters for which sloughing events are significant. The value of k_{det} = 9.5 m^{-1} h^{-1} chosen for these 2D replicate simulations produces a biofilm for which sloughing contributes approximately 25% of total biomass detachment (derived from the values in Table 2). Results show a strong resemblance to those reported for biofilms

grown in flat plate reactors (Lewandowski *et al.*, 2004). Namely, this resemblance is patent in the presence of a predictable initial development stage, lasting until the occurrence of the first sloughing event, which is then followed by cycles of growth–sloughing–regrowth of an apparently unpredictable nature. From the 2D simulations reported here, it is observed that, in the long run, the apparently unpredictable dynamics of the growth–sloughing–regrowth cycles constitutes a "noisy" steady state. Furthermore, the characteristics of this steady state are well reproduced by replicate simulations carried out using different seeds for the random number generator. These results suggest that the fact that no absolute steady state is observed for the structure at the microscale does not exclude the existence of a steady state at the reactor scale. In order to observe the "noisy" steady state, however, biofilm growth may have to be monitored for long periods. Lewandowski *et al.* (2004) monitored biofilm growth for up to 35 days, which in total corresponds to 175% of the "predictable" initial development period observed of about 20 days. This monitoring period is possibly too short to assess the existence of a "noisy" steady state. In fact, Lewandowski *et al.* (2004) are aware of this possibility, as stated in the discussion section of their report. There, they hypothesize that these growth–sloughing–regrowth cycles may in fact be reproducible. The replicate simulations described here represent biofilm growth for up to 166 days, more than 660% of the initial development period of about 25 days, a period shown to be sufficient to observe the occurrence and reproducibility of a "noisy" steady state. This suggests a possible new use of multi-dimensional modelling approaches, such as the 2D IbM used here, to assist on the design of experiments relying on biofilm structure reproducibility.

Trends in steady-state structure

Picioreanu *et al.* (1998) proposed the dimensionless *G* ("growth") group to describe not only the relative effects of transport and reaction of a growth limiting solute as the Thiele modulus does in chemical engineering, but also the capability of the active biofilm layer to generate volume:

$$G = \frac{\text{maximum biomass growth rate}}{\text{maximum substrate transport rate}} = L_f^2 \frac{\mu^{max} C_H}{D_O C_O^{bulk}} \quad \text{[dimensionless]} \quad (12)$$

In the same study, the roughness of a biofilm grown unrestrictedly, i.e. with no detachment present, obtained from 2D and 3D simulations was shown to be related to the value of *G*. Biofilm systems with high *G* values, indicating fast biomass spreading relative to the transport rate of a growth-limiting solute, developed porous and irregular biofilms, whereas growth at low *G* values produced smooth and compact biofilms. Using a linear analysis of a continuum biofilm model also considering unrestricted biofilm growth, Dockery & Klapper (2001) showed that roughness in a quasi-flat biofilm may arise when growth-induced instabilities are of wavelengths of the length scale of the penetration depth of a growth-limiting substrate. In both these studies it was observed that instabilities in the biofilm surface, once formed, are self-enhancing. The tips of the finger-like clusters, being at the top of the biofilm, experience higher concentrations of the growth-limiting substrate and thus grow faster relatively to the remaining biomass.

These results demonstrate the importance of the penetration depth of a growth-limiting substrate. More generally, they demonstrate the relevance of the solute gradients in the creation of rough biofilms. Other modelling approaches have shown similar results while including other forms of detachment mechanism (Hermanowicz, 2001; Picioreanu *et al.*, 2001; Chang *et al.*, 2003).

In natural and industrial systems, detachment is the main mechanism balancing biomass growth (Stewart, 1993). The prevailing factor conditioning biofilm structure is a balance of the mass transport regimen of a growth-limiting solute and detachment (Van Loosdrecht *et al.*, 1995). The importance of detachment on the biofilm structure and activity in the steady state is clear in the results shown for 2D simulations carried for a range of k_{det} values (shown in Figs. 5 and 6). All biofilm parameters are kept constant in these simulations, which means that both the *G* number and Thiele modulus are also the same. In spite of this, a range of biofilm structures may still be obtained (as shown in Fig. 6e), as concluded also in the modelling study of Picioreanu *et al.* (2001).

The fact that biofilm activity decreases with the occurrence of surface heterogeneity, as discussed previously both in modelling studies (Eberl *et al.*, 2000; Picioreanu *et al.* 2000; Klapper, 2004) and experimental reports (Wasche *et al.*, 2000), is very relevant for the operation of biofilm reactors. This decrease in biofilm activity (here defined as the biomass production rate) is shown in Figs. 6c and 7c, in which rates of biomass production predicted by the 2D models are lower than those obtained from both 1D models, particularly when 2D structures are porous and have a rough shape. Results from zero-order and Monod-type kinetics 1D models are generally in agreement, suggesting that deviations from zero-order kinetics are not significant for this system. As 1D approaches have in common the assumption of a planar geometry, agreement between 1D and 2D occurs only for the cases where biofilm morphology predicted by 2D is smooth and planar. This is the case where applied erosion is highest (Fig. 6C) and maximum specific growth rates of organisms are lower (Fig. 7c). The 1D and 2D results diverge the most for cases where steady-state porosity is very high, which is the result of heterogeneous biofilm structure. Fig. 5 well illustrates this trend by showing very good agreement of biofilm thickness from 1D and 2D models for the case where k_{det} is highest, and decreasing agreement as k_{det} values become lower, as a consequence of the increasing heterogeneity of the biofilm formed. Results from 2D simulations presented in Fig. 7c further show the important trend that the overall biofilm activity decreases with increasing μ^{max} of microorganisms. This trend is in total disagreement with results from 1D models that predict that biofilm activity (biomass production rate)

should increase, albeit slightly, with increasing μ^{max}. These divergences between 1D and 2D results are accounted for by three main factors: (1) the increase in biofilm porosity and surface roughness (due to diffusional limitation), which constitute a reduction of the biomass concentration at the top of the biofilm where the biofilm is more active; (2) an increase in biofilm surface area for rough biofilms, which increases the exposure to detachment forces; and (3) the occurrence of sloughing events, the relative importance of which is observed to increase for rough biofilms. These three effects may be derived only from simulations of dimensionality higher than 1D, which clearly illustrates the relevance of using multi-dimensional (2D or 3D) models.

CONCLUSIONS

A simple model of biofilm growth and detachment with a single heterotrophic species and a single solute species (oxygen) was used for 2D simulations with results describing trends for activity and structure of biofilms observed experimentally in biological reactors.

Replicate simulations show that the existence and reproducibility of a steady state may also occur in cases where the occurrence of sloughing events of an apparently random nature constitutes a significant fraction of the overall biomass detachment. However, in order to observe these "noisy" steady states, both in simulations and experimentally, biofilm growth may have to be followed for long periods.

Biofilm morphology derived from 2D simulations illustrates the importance of the mass transport regimen of a growth-limiting solute, which may be quantified by dimensionless values such as the G number or the Thiele modulus, but also of the applied detachment forces.

When compared with 2D simulation results, 1D models show good agreement for cases where biofilm morphology predicted by 2D is planar, such as the cases of high applied erosion forces and low maximum specific growth rates (μ^{max}). However, large differences are observed when the structure predicted by the 2D model is heterogeneous, including significant decreases in biofilm activity and the occurrence of sloughing events, effects that 1D modelling approaches are not able to describe implicitly.

ACKNOWLEDGEMENTS

J. B. Xavier thankfully acknowledges financial support by the F.C.T./M.C.T.E.S., Portugal, through the grant SFRH/BPD/11485/2002.

APPENDIX: ANALYTICAL SOLUTION OF STEADY STATE FOR ZERO-ORDER KINETICS

By assuming zero-order kinetics (valid for $G_O \gg K_O$), the local rate of oxygen consumption, derived from equations 2 and 3, becomes

$$R_O = -Y_{OH}\mu^{max}C_H \qquad [M_O L^{-3}T^{-1}] \qquad (13)$$

For this case, a critical depth δ exists below which the concentration of oxygen is zero. The thickness of this active layer is determined in relation to the oxygen concentration at the biofilm–liquid interface (C_O^{surf}) by

$$\delta = \sqrt{\frac{2D_O C_O^{surf}}{Y_{OH}\mu^{max}C_H}} \qquad [L] \qquad (14)$$

(Pérez *et al.*, 2004). At the liquid side of the interface, the flux of oxygen is defined using an external mass transfer resistance

$$J_O^{liquid} = k_L\left(C_O^{bulk} - C_O^{surf}\right) \qquad [M_O L^{-2}T^{-1}] \qquad (15)$$

At the biofilm side, the flux is

$$J_O^{biofilm} = \sqrt{2D_O Y_{OH}\mu^{max}C_O^{surf}C_H} \qquad [M_O L^{-2}T^{-1}] \qquad (16)$$

The flux of oxygen at both sides of the biofilm–liquid interface must have equal values, i.e. $J_O^{liquid} = J_O^{biofilm}$, which provides a solution for C_O^{surf}. By defining a Thiele modulus as

$$\phi_O^2 = \frac{2D_O Y_{OH}\mu^{max}C_H}{k_L^2 C_O^{bulk}} \qquad [\text{dimensionless}] \qquad (17)$$

The oxygen concentration at the biofilm–liquid interface becomes

$$C_O^{surf} = C_O^{bulk}\left[\frac{-\phi_O + \sqrt{\phi_O^2 + 4}}{2}\right]^2 \qquad [M_O L^{-3}] \qquad (18)$$

Equation 18 is one of the two solutions of the quadratic equation that results from equations 15 and 16. From those

Table 3: Steady-state biofilm properties for zero-order kinetics, directly derived from the value of δ

Property	Steady-state expression[a]	Dimensions	Derivation
Biofilm thickness, L_f	$L_f = \sqrt{\frac{\delta\mu^{max}}{k_{det}}}$ (19)	L	Solving equation 6
Detachment rate	$R_{det,ss} = C_H(\delta\mu^{max})^2$ (20)	$M_H L^{-2}T^{-1}$	Using $L_{f,ss}$ in equation 1
Average solids retention time	$SRT_{ss} = \frac{1}{\sqrt{k_{det}\delta\mu^{max}}}$ (21)	T	The ratio of steady state biomass in biofilm ($L_{f,ss}C_H$) and $R_{det,ss}$
Overall oxygen consumption rate	$R_O = Y_{OH}\mu^{max}C_H\delta$ (22)	$M_O L^{-2}T^{-1}$	The maximum specific oxygen consumption rate ($Y_{OH}\mu^{max}$) multiplied by the biomass in the active layer

[a] Numbers in parentheses are expression numbers referred to in the text.

Table 4: Nomenclature

Symbol	Definition	Dimensions
ε	Biofilm porosity (volume of voids divided by total volume, the average of areal porosity, ε_A, along the entire depth of the biofilm)	—
ε_{A}	Areal porosity of the biofilm (used in areal porosity profiles)	—
δ	Oxygen penetration depth or thickness of biofilm active layer	L
$\mu^{\max}$	Maximum specific growth rate of microorganisms	T^{-1}
ρ_{H}	Specific mass of heterotrophic biomass	$\mathrm{M_H L}^{-3}$
ϕ_{O}	Zero-order kinetics Thiele modulus (defined in equation 17)	—
$C_{\mathrm{O}}^{\mathrm{bulk}}$	Concentration of oxygen in the bulk liquid	$\mathrm{M_O L}^{-3}$
$C_{\mathrm{O}}^{\mathrm{surf}}$	Concentration of oxygen at the biofilm surface	$\mathrm{M_O L}^{-3}$
C_{H}	Biomass concentration in biofilm	$\mathrm{M_H L}^{-3}$
D_{O}	Diffusivity coefficient of oxygen	$\mathrm{L}^2\mathrm{T}^{-1}$
F_{det}	Detachment speed function	LT^{-1}
G	Dimensionless growth number	—
k_{det}	Detachment speed coefficient	$\mathrm{L}^{-1}\mathrm{T}^{-1}$
K_{O}	Monod saturation constant for oxygen	$\mathrm{M_O L}^{-3}$
L_{bl}	Thickness of concentration boundary layer	L
L_{f}	Maximum biofilm thickness	L
$L_{\mathrm{f,ss}}$	Steady-state biofilm thickness	L
L_z	Depth of 2D system (defined for mass conservation purposes)	L
M_{p}	Mass of heterotrophic biomass in a biomass particle (agent)	$\mathrm{M_H\ particle}^{-1}$
$R_{\mathrm{det,ss}}$	Steady-state detachment rate of biofilm	$\mathrm{L}^3\mathrm{T}^{-1}$
R_{division}	Critical radius for biomass particle (agent) division	L
R_{O}	Oxygen consumption rate	$\mathrm{M_O L}^{-3}\mathrm{T}^{-1}$
R_{H}	Biomass production rate	$\mathrm{M_H L}^{-3}\mathrm{T}^{-1}$
R_{p}	Radius of a particle ("agent")	$\mathrm{M_H}$
$\mathrm{SRT_{ss}}$	Solids retention time at steady state	T
Y_{OH}	Yield of oxygen consumed per biomass produced	$\mathrm{M_O M_H}^{-1}$

two solutions, only equation 18 is valid, as it produces values where $C_{\mathrm{O}}^{\mathrm{surf}} \leq C_{\mathrm{O}}^{\mathrm{bulk}}$, a relation that must be observed, since oxygen is not produced in the biofilm. Together, equations 14 and 18 allow the value of the thickness of the active layer (δ) to be determined. For zero-order kinetics, δ defines all steady-state characteristics for a given biofilm such as the steady-state biofilm thickness, the detachment rate, the solids retention time (SRT) and the activity of the biofilm defined in terms of oxygen consumed per area of carrier surface. Equations for deriving several parameters from the value of δ are given in Table 3. A list of the nomenclature used in these studies is given in Table 4.

REFERENCES

Beun, J. J., Dircks, K., Van Loosdrecht, M. C. M. & Heijnen, J. J. (2002) Poly-beta-hydroxybutyrate metabolism in dynamically fed mixed microbial cultures. *Water Research* **36**, 1167–1180

Bryers, J. D. & Characklis, W. G. (1982) Processes governing primary biofilm formation. *Biotechnology and Bioengineering* **24**, 2451–2476

Chang, I., Gilbert, E. S., Eliashberg, N. & Keasling, J. D. (2003) A three-dimensional, stochastic simulation of biofilm growth and transport-related factors that affect structure. *Microbiology-sgm* **149**, 2859–2871

Davies, D. G., Parsek, M. R., Pearson, J. P., Costerton, J. W. & Greenberg, E. P. (1998) The involvement of cell-to-cell signals in the development of a bacterial biofilm. *Science* **280**, 295–298

Dockery, J. & Klapper, I. (2001) Finger formation in biofilm layers. *SIAM Journal of Applied Mathematics* **62**, 853–869

Eberl, H. J., Picioreanu, C., Heijnen, J. J. & Van Loosdrecht, M. C. M. (2000) A three-dimensional numerical study on the correlation of spatial structure, hydrodynamic conditions, and mass transfer and conversion in biofilms. *Chemical Engineering Science* **55**, 6209–6222

Gjaltema, A., Tijhuis, L., Van Loosdrecht, M. C. M. & Heijnen, J. J. (1995) Detachment of biomass from nongrowing spherical biofilms in airlift reactors. *Biotechnology and Bioengineering* **46**, 256–269

Heijnen, J. J., Van Loosdrecht, M. C. M., Mulder, R., Weltevrede, R. & Mulder, A. (1993) Development and scale-up of an aerobic biofilm airlift suspension reactor. *Water Science and Technology* **27**(5–6), 253–261

Hermanowicz, S. W. (2001) A simple 2D biofilm model yields a variety of morphological features. *Mathematical Biosciences* **169**, 1–14

Heydorn, A., Ersbøll, B. K., Hentzer, M., Parsek, M. R., Givskov, M. & Molin, S. (2000) Experimental reproducibility in flow-chamber biofilms. *Microbiology* **146**, 2409–2415

Jackson, G., Beyenal, H., Rees, W. M. & Lewandowski, Z. (2001) Growing reproducible biofilms with respect to structure and viable cell counts. *Journal of Microbiological Methods* **47**, 1–10

Klapper, I. (2004) Effect of heterogeneous structure in mechanically unstressed biofilms on overall growth. *Bulletin of Mathematical Biology* **66**, 809–824

Kreft, J. U., Picioreanu, C., Wimpenny, J. W. T. & Van Loosdrecht, M. C. M. (2001) Individual-based modelling of biofilms. *Microbiology-sgm* **147**, 2897–2912

Kwok, W. K., Picioreanu, C., Ong, S. L., Van Loosdrecht, M. C. M., Ng, W. J. & Heijnen, J. J. (1998) Influence of biomass production and detachment forces on biofilm structures in a biofilm airlift suspension reactor. *Biotechnology and Bioengineering* **58**, 400–407

Levenspiel, O. (1972) *Chemical Reactor Engineering*, New York: Wiley

Lewandowski, Z. (2000) Notes on biofilm porosity. *Water Research* **34**, 2620–2624

Lewandowski, Z., Beyenal, H. & Stookey, D. (2004) Reproducibility of biofilm processes and the meaning of steady state in biofilm reactors. *Water Science and Technology* **49**(11), 359–364

Morgenroth, E. & Wilderer, P. A. (2000) Influence of detachment mechanisms on competition in biofilms. *Water Research* **34**, 417–426

Pérez, J., Picioreanu, C. & Van Loosdrecht, M. C. M. (2005) Modeling biofilm and floc diffusion processes based on analytical solution of reaction–diffusion equations. *Water Research*, in press

Picioreanu, C., Van Loosdrecht, M. C. M. & Heijnen, J. (1998) Mathematical modelling of biofilm structure with a hybrid differential–discrete cellular automaton approach. *Biotechnology and Bioengineering* **58**, 101–116

Picioreanu, C., Van Loosdrecht, M. C. M. & Heijnen, J. J. (2000) A theoretical study on the effect of surface roughness on mass transport and transformation in biofilms. *Biotechnology and Bioengineering* **68**, 355–369

Picioreanu, C., Van Loosdrecht, M. C. M. & Heijnen, J. J. (2001) Two-dimensional model of biofilm detachment caused by internal stress from liquid flow. *Biotechnology and Bioengineering* **72**, 205–218

Picioreanu, C., Kreft, J. U. & Van Loosdrecht, M. C. M. (2004a) Particle-based multidimensional multispecies model. *Applied and Environmental Microbiology* **70**, 3024–3040

Picioreanu, C., Xavier, J. B. & van Loosdrecht, M. C. M. (2004b) Advances in mathematical modeling of biofilm structure. *Biofilms* **1**, in press

Purevdorj, B., Costerton, J. W. & Stoodley, P. (2002) Influence of hydrodynamics and cell signaling on the structure and behavior of *Pseudomonas aeruginosa* biofilms. *Applied and Environmental Microbiology* **68**, 4457–4464

Reichert, P. (1994) Aquasim – a tool for simulation and data-analysis of aquatic systems. *Water Science and Technology* **30**(2), 21–30

Rittmann, B. E., Pettis, M., Reeves, H. W. & Stahl, D. A. (1999) How biofilm clusters affect substrate flux and ecological selection. *Water Science and Technology* **39**(7), 99–105

Rittmann, B. E., Schwarz, A. O., Eberl, H. J., Morgenroth, E., Perez, J., van Loosdrecht, M. & Wanner, O. (2004) Results from the multi-species benchmark problem (BM3) using one-dimensional models. *Water Science and Technology* **49**(11–12), 163–168

Saez, P. B. & Rittmann, B. E. (1992) Accurate pseudoanalytical solution for steady-state biofilms. *Biotechnology and Bioengineering* **39**, 790–793

Sethian, J. A. (1996) A fast marching level set method for monotonically advancing fronts. *Proceedings of the National Academy of Sciences, USA* **93**, 1591–1595

Stewart, P. S. (1993) A model of biofilm detachment. *Biotechnology and Bioengineering* **41**, 111–117

Stoodley, P., Sauer, K., Davies, D. G. & Costerton, J. W. (2002) Biofilms as complex differentiated communities. *Annual Review of Microbiology* **56**, 187–209

Tijhuis, L., Hijman, B., Van Loosdrecht, M. C. M. & Heijnen, J. J. (1996) Influence of detachment, substrate loading and reactor scale on the formation of biofilms in airlift reactors. *Applied Microbiology and Biotechnology* **45**, 7–17

Tijhuis, L., Van Loosdrecht, M. C. M. & Heijnen, J. J. (1994) Formation and growth of heterotrophic aerobic biofilms on small suspended particles in airlift reactors. *Biotechnology and Bioengineering* **44**, 595–608

Van Loosdrecht, M. C. M., Eikelboom, D., Gjaltema, A., Mulder, A., Tijhuis, L. & Heijnen, J. J. (1995) Biofilm structures. *Water Science and Technology* **32**(8), 35–43

Villaseñor, J. C., Van Loosdrecht, M. C. M., Picioreanu, C. & Heijnen, J. J. (2000) Influence of different substrates on the formation of biofilms in a biofilm airlift suspension reactor. *Water Science and Technology* **41**(4–5), 323–330

Wanner, O. & Gujer, W. (1986) A multispecies biofilm model. *Biotechnology and Bioengineering* **28**, 314–328

Wanner, O. & Reichert, P. (1996) Mathematical modeling of mixed-culture biofilms. *Biotechnology and Bioengineering* **49**, 172–184

Wasche, S., Horn, H. & Hempel, D. C. (2000) Mass transfer phenomena in biofilm systems. *Water Science and Technology* **41**(4–5), 357–360

Wasche, S., Horn, H. & Hempel, D. C. (2002) Influence of growth conditions on biofilm development and mass transfer at the bulk/biofilm interface. *Water Research* **36**, 4775–4784